ACS Energy LETTERS

http://pubs.acs.org/journal/aelccp

LETTER

Persistent Photoconductivity in Perylene Diimide Nanofiber Materials

Na Wu,[†] Chen Wang,[†] Paul M. Slattum,[‡,§] Yaqiong Zhang,[†] Xiaomei Yang,[†] and Ling Zang*[,†]

[†]Nano Institute of Utah and Department of Materials Science and Engineering, University of Utah, 36 South Wasatch Drive, Salt Lake City, Utah 84112, United States

[‡]Vaporsens Inc., 36 South Wasatch Drive, Salt Lake City, Utah 84112, United States

[§]Leibniz-Institut für Polymerforschung Dresden e.V., Hohe Straße 6, D-01069 Dresden, Germany

Supporting Information

ABSTRACT: **Perylene tetracarboxylic diimide (PTCDI) derivatives have been extensively investigated for one-dimensional (1D) self-assembly and their applications in optoelectronic devices. Our study on self-assembled PTCDI nanofiber materials revealed a persistent photoconductivity (PPC) effect, which is sustained conductivity after illumination is terminated. A comprehensive understanding of the PPC effect in PTCDI nanofibril materials will enable us to explore and enhance their optoelectronic applications. Here, we have investigated the PPC effect in the nanofibers assembled from 1-methylpiperidine-substituted perylene tetracarboxylic diimide (MP-PTCDI) with respect to the PPC relaxation at different temperatures, illumination power densities, molar amount, and morphology of the PTCDI film deposited on the interdigitated electrodes. The photocurrent relaxation was also performed on several other PTCDI nanofiber materials for comparative study. We conclude that the significant PPC effect in MP-PTCDI nanofibers can be attributed to the electrical potential fluctuations caused by the structure defects, which thus hinder the recombination of charge carriers. This study may provide new design rules for fabrication of molecular semiconductor materials with strong PPC in order to approach high efficiency of photovoltaics and photocatalysis.**

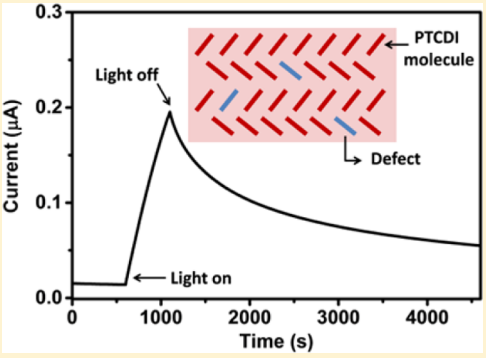

Perylene tetracarboxylic diimide (PTCDI) derivatives, forming a typical n-type organic semiconductor, have been receiving much research attention because of their high thermal- and photostability.[1,2] Their strong electron affinity and strong absorption in the visible light region make PTCDI a good candidate for next-generation photovoltaic devices[3−6] and photocatalytic materials.[7,8] In addition, self-assembly of PTCDI molecules often gives rise to the formation of well-defined nanofibril structures through the columnar $\pi-\pi$ stacking between the perylene planes.[2] The as-prepared PTCDI nanofibers assist in the construction of the distinctive morphology of p−n junction nanostructures in photovoltaic devices to improve their performance,[4,6] for instance, the novel crystalline donor/acceptor (P3HT/PTCDI) shish-kebab structure,[4,9] in which the observed high photovoltage was likely due to this special intermolecular orientation. PTCDI nanofibril materials have the potential to be used in photocatalytic systems as well. Previous research has shown that PTCDI molecules with attached donor moieties were self-assembled into nanofibers, followed by coating with cocatalysts, such as TiO_2 and/or Pt,[7,8] or g-C_3N_4 and Pt,[10] showed excellent performance in the photocatalytic splitting of water for H_2 production. The excellent photocatalytic activity of the composite photocatalysts was attributed to PTCDIs' strong visible light absorption, matched energy level, and effective charge separation with the cocatalysts.[7,8]

In this study, persistent photoconductivity (PPC), which is sustained conductivity after illumination is terminated,[11] was observed by accident in the nanofibers fabricated from a PTCDI molecule with a donor−acceptor (D−A) structure [1-methylpiperidine substituted-PTCDI molecule (MP-PTCDI) shown in Scheme 1]. In general, the PPC effect is not so commonly observed in organic semiconductor materials as in inorganic counterparts. For PTCDI-based materials there have been few reports where the PPC effect was implied.[12,13] We believe that further study of the PPC effect and the dependence on materials structure will offer deep insight into the charge carrier storage and relaxation process within organic semiconductor materials (particularly PTCDIs), thus providing guidance in optimizing the photovoltaic and photocatalytic performance of these materials.

The PPC effect has been mostly observed and investigated in inorganic semiconductor compounds, alloys, and heterojunc-

Received: September 8, 2016
Accepted: October 7, 2016
Published: October 7, 2016

DOI: 10.1021/acsenergylett.6b00422
ACS Energy Lett. 2016, 1, 906−912

Scheme 1. Molecular Structures of PTCDI Building Blocks Used in This Study

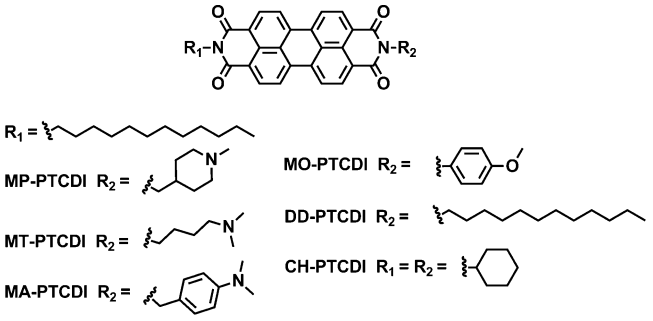

tions.[11,14−18] Generally, the PPC effect is caused by a potential barrier that prohibits the recombination of photogenerated electron−hole pairs. There are multiple models to describe the PPC mechanism in regard to various material systems, such as random localized potential fluctuations (RLPF), large lattice relaxation (LLR), and microscopic barrier (MB).[11] In the RLPF model, carriers are separated by the potential fluctuations, which reduce the rate of recombination, producing PPC. For example, RLPF induced by composition fluctuation was found to be responsible for PPC observed in $Zn_{0.3}Cd_{0.7}Se$ mixed crystals[14] and $CdS_{0.5}Se_{0.5}$ semiconductor alloy.[16] In addition to the intrinsic sources, extrinsic origins of RLPF may also come from the substrate effect as was found in monolayer MoS_2 field effect transistors.[11] In a LLR model, deep-level traps (DX centers) are considered to be the source of PPC. Under illumination, the DX center can be converted into a metastable shallow donor state, which produces a potential barrier due to the difference in lattice relaxation between the two states. The recapture of electrons by the DX center is prevented by the barrier, leading to the PPC effect.[18,19] The LLR model was supported by a study on n-type $Al_xGa_{1-x}As$, for which the PPC effect was produced by donor-related defects.[19] The MB model is based on the spatial macroscopic potential barrier, which separates the photoexcited electron−hole pairs, and this model explains well the PPC effect in many heterostructures, such as graphene/MoS_2,[17] quantum-dot/graphene,[20] and chlorophyll/graphene.[21]

Although the PPC effect and its influence on optoelectronic properties and performance have been extensively studied on the inorganic semiconductors, such detailed study on the organic materials is lacking. Especially, most of the PPC studies have been performed at low temperatures (e.g., from 17 to 300 K).[15] Room-temperature study of the PPC within organic materials would fill in the field with new knowledge by understanding better the sustained photoinduced charge separation.[22−24] In this work, an electron donor−acceptor PTCDI, MP-PTCDI (Scheme 1), was chosen as the organic semiconductor material to study the PPC effect. For comparison, several other PTCDIs were also employed and investigated in parallel under the same conditions. Moreover, the PTCDIs form well-defined nanofibers through solution-phase self-assembly, and the one-dimensional (1D) intermolecular arrangement (dominated by the cofacial $\pi-\pi$ stacking) provides an efficient charge-transport pathway, which further

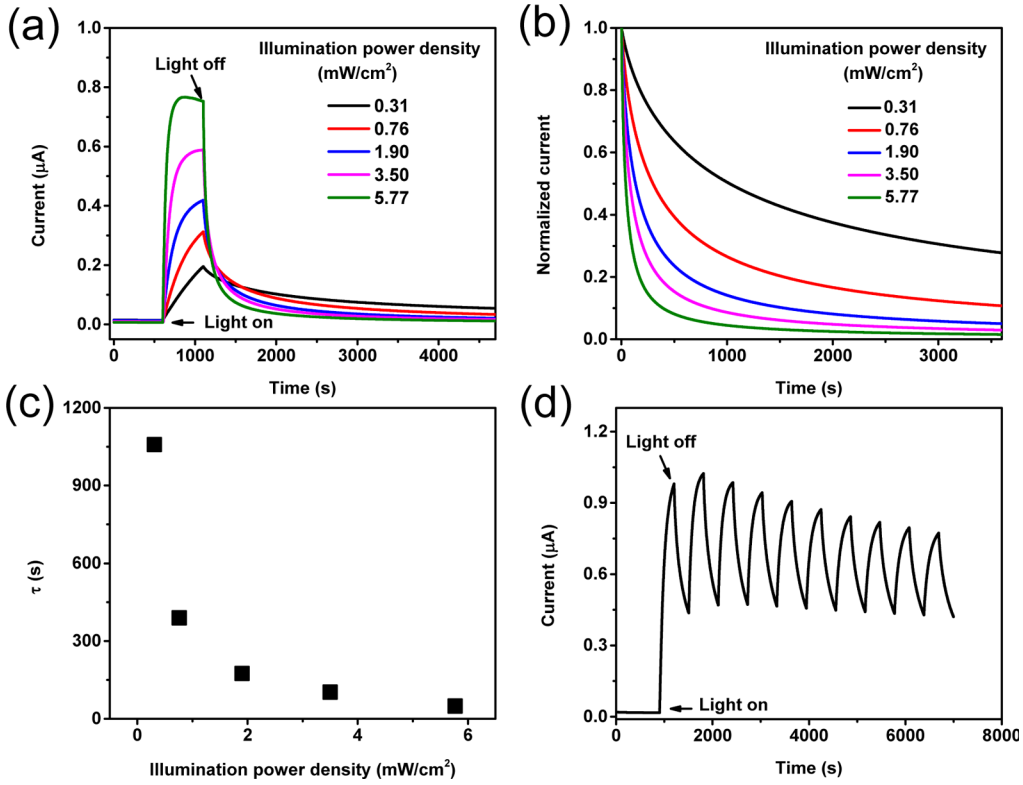

Figure 1. (a) Photocurrent response of MP-PTCDI nanofibers under ambient conditions with various white light illumination power densities. (b) Decay of the photocurrent in panel a (normalized) generated at different illumination power densities after removal of the light. (c) Photocurrent decay time constant (τ) as a function of illumination power density. (d) Multicycle photocurrent response of the MP-PTCDI nanofibers by repeatedly switching on and off the illumination (3.50 mW cm^{-2}) in a 300 s interval. All the measurements were under the bias voltage of 7 V.

DOI: 10.1021/acsenergylett.6b00422
ACS Energy Lett. 2016, 1, 906−912

enhances the charge separation and is suited for application in photocatalysis and photovoltaics.[25] As observed in this study, the PPC decay time of MP-PTCDI nanofibers can be as long as 1058 s. The PPC decay was found to be dependent on the temperature, irradiation power density, film morphology, and amount of nanofibers deposited on the interdigitated electrodes (IDE). Moreover, the side groups of PTCDI can be modified with electron-donating moieties with different donation power (as shown in Scheme 1) in order to investigate the influence of electron donor−acceptor interaction on the PPC. Donor−acceptor interaction, particularly under photoexcitation, creates charge separation and electrostatic traps, thus producing potential barriers that hinder the recombination of electron−hole pairs. Because the two imide positions within PTCDI are nodes in the π-orbitals, changing the substitutions at the two ends does not change significantly the electronic properties of PTCDI.[25,26] This enabled us to perform the comparative PPC studies employing different PTCDI molecules shown in Scheme 1, from which the effect of the electron-donating group can be investigated.

Figure 1 shows the PPC results obtained with the MP-PTCDI nanofibers deposited on IDEs. After maintaining a stable current in the dark, the MP-PTCDI nanofibers were then illuminated by white light with a spot size covering the whole nanofiber area. The nanofibers demonstrated high photoconductivity upon illumination, producing a photocurrent on/off ratio ranging from ca. 18 to 71 with the illumination power density increasing from 0.31 to 5.77 mW cm^{-2} under a bias voltage of 7 V (Figure 1a and Table S1). After termination of illumination, the photocurrent relaxed quite slowly to the dark current level, and the decay rate depends significantly on the illumination power density (Figure 1b). The PPC decay curves can be well-fitted by a single stretched exponential decay (eq 1), namely Kohlrausch's law, as widely reported in the literature on PPC effect[11,14]

$$I_{(t)} = I_0 \exp[-(t/\tau)]^{\beta} \quad (0 < \beta < 1) \tag{1}$$

where I_0 is the photocurrent before the illumination is removed; τ is the decay time constant, representative of the time scale of the decay process, and β is the deviation from a single-exponential decay. The decay time constant (τ) of the MP-PTCDI nanofibers under illumination with various illumination power densities are shown in Figure 1c and summarized in Table S1. It is noted that the decay time constant decreases with the increase of illumination power density. When the illumination power density increases, a higher concentration of free charger carriers should be produced within the MP-PTCDI nanofibers,[12,25,27] as evidenced by the increased photocurrent on/off ratio and the shorter time required for achieving photocurrent equilibrium (Table S1). The higher concentration of free charge carriers leads to a greater probability of recombination of charge carriers and consequently faster decay of the photocurrent. The PPC observed with the MP-PTCDI nanofibers was also found reproducible as confirmed by cycling on and off the illumination in 300 s intervals (Figure 1d). When the light was turned on, the current increased rapidly. Upon termination of the illumination, the current dropped to about 50% of the photocurrent within 300 s in the first cycle, and this "on" and "off" photoswitching remained reversible and reproducible in the following cycles. The lowest current obtained at 300 s after the termination of light still stays at the level of about 50% of the maximal photocurrent generated in the first cycle, though the photocurrent generated in the later cycles drifted lower to some extent, likely due to the photooxidation,[27−30] as the experiments were run in air.

We also observed the wavelength dependence of the photoconductivity and PPC effect of MP-PTCDI nanofiber materials by using long-pass filters with cut-on wavelength of 550 and 700 nm, while keeping the flux of photons constant in both cases. As shown in Figure S3, with the 550 nm filter, the photocurrent on−off ratio obtained for MP-PTCDI nanofibers was ca. 19 and a significant PPC effect was observed with decay time of 269 s, whereas when a 700 nm filter was used, there was no photoconductivity obtained for the same nanofibers, simply because the wavelength above 700 nm has less than the band gap energy to initiate the highest occupied molecular orbital−lowest unoccupied molecular orbital transition of PTCDI.[27]

As extensively investigated with GaN, the PPC effect was found to be structure-dependent.[31,32] For example, when fabricated as nanorods, the PPC effect of GaN was strongly related to the diameter of nanorods,[31] and a further enhanced PPC was observed in nanoporous GaN formed by electrochemical etching.[32] Inspired by such research work on inorganic materials, we attempted to study how the structure (morphology) of MP-PTCDI materials would affect the PPC as observed in Figure 1. Taking advantage of the ease of molecular self-assembly of PTCDIs, the morphology of MP-PTCDI materials can be controlled via evaporation-induced molecular assembly on the oxidized surface of silicon wafer (or silicon wafer prepatterned with IDEs). Such an in situ fabrication method allowed us to tune the morphology of molecular aggregates through thermal and solvent vapor annealing (see experimental details in the Supporting Information).[33] The AFM images in Figure 2 indicate the evolution of the MP-PTCDI nanofiber structure from the initially disordered particulate aggregate under different annealing processes. The drop-cast thin film formed directly from the evaporation in air showed partially dewetted patterns, and there was no obvious structure or ordered morphology (Figure 2a). When the sample was annealed at 60 °C for 72 h, an approximately uniform and worm-shaped pattern formed in the film (Figure 2b). Upon annealing in the vapor of ethanol (a poor solvent for MP-PTCDI) for 24 h, well-defined nanofiber structures were established (Figure 2c), where the dimensions of the nanofibers is about 500−800 nm in length and 200 nm in width. We investigated the PPC effect with the three MP-PTCDI thin films annealed under different conditions, and the results are shown in Figure 2d. The as-prepared thin film shows the fastest decay in current (with τ = 53 ± 3 s), followed by the film thermally annealed at 60 °C (τ = 93 ± 6 s), and the nanofiber film annealed in ethanol vapor shows the slowest decay (τ = 119 ± 10 s). Clearly, the self-assembled 1D nanostructure with the most organized molecular packing through π−π stacking enhances the PPC effect in MP-PTCDI.

The PPC was also found to be dependent on the molar amount of MP-PTCDI nanofibers deposited on the IDEs. The decay time constant increased with the molar amount of nanofibers, while the rate of increase slowed when more than 1 nmol of nanofibers were deposited, mainly because the efficient conductive channel of MP-PTCDI nanofibers becomes saturated on the IDEs used (Figure S4). We also investigated the PPC in a control sample, in which MP-PTCDI nanofibers were dispersed in a PEG−PPG−PEG polymer matrix. When the nanofibers were dispersed in a polymer matrix, the

DOI: 10.1021/acsenergylett.6b00422
ACS Energy Lett. 2016, 1, 906−912

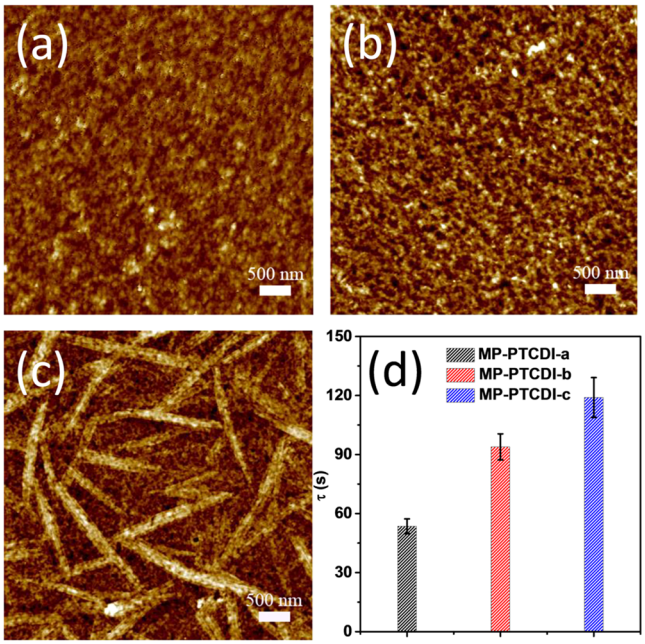

Figure 2. AFM images of MP-PTCDI thin film drop-cast on silicon wafer after consequent treatments: (a) dried in air for 1 h, (b) aged at 60 °C for 72 h, and (c) annealed in ethanol vapor for 24 h. (d) Comparison of the PPC decay time constant (τ) of the MP-PTCDI thin film deposited on silicon wafer prepatterned with IDEs formed in panels a, b, and c. The error bars represent the standard deviation based on the values measured by three independent devices of each condition. The irradiation power density was 3.50 mW cm^{-2}. The bias voltage was 7 V.

interfiber contact would be insulated by the polymer, thus excluding the possibility that the interfiber contact (junction) may contribute to the observed PPC. As expected, the average width of the fibers is now 200 nm greater than the value of pristine MP-PTCDI nanofibers because of the surface coating of polymers (Figure S5). The almost identical PPC observed in the control sample (Figure S6, the decay time of 103 and 102 s for the pristine MP-PTCDI nanofibers and those embedded in polymer, respectively) suggested negligible contribution from the junctions of nanofibers. The origin of the PPC effect should be correlated to nanofiber structure and the 1D crystal lattice.

To further explore the mechanism of the observed PPC effect in the MP-PTCDI nanofibers, a series of other PTCDI molecules with different side groups were studied for comparison. Most of these PTCDIs contain a linear dodecyl chain on one side but have different groups on the other side; CH-PTCDI is the only symmetric molecule with both sides substituted with a cyclohexane group (Scheme 1). All these PTCDIs were fabricated into nanofibers following the similar self-assembly process and investigated for the PPC under the same conditions as used for MP-PTCDI nanofibers. Interestingly, PPC was found only in the nanofibers fabricated from the PTCDIs substituted with strong electron-donating groups, such as MP-PTCDI, MT-PTCDI, and MA-PTCDI (Figure 3), where the PPC decay curves can be fitted with a single stretched exponential equation, as widely reported in the literature on PPC effect,[11,14] although the whole decay has a long tail that takes more than 1 h to reach the dark current baseline. In contrast, no significant PPC effect was observed for the nanofibers of PTCDIs with weak electron donors (e.g., MO-PTCDI, DD-PTCDI, and CH-PTCDI), for which the

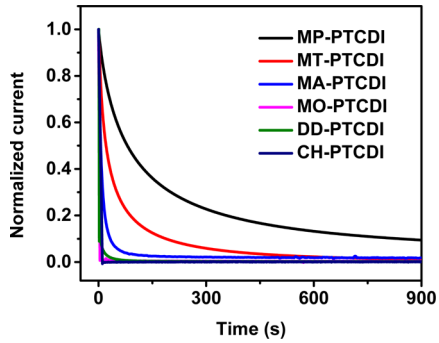

Figure 3. PPC relaxation curves of various PTCDI nanofibril materials at room temperature. The irradiation power density was 3.50 mW cm^{-2}. The bias voltage was 7 V. The data were normalized to the photocurrent value right before turning off the light for each PTCDI nanofiber in order to compare the decay kinetics.

photocurrent returned relatively quickly to the dark current level in less than 10 s, and the PPC decay curves of which do not fit into the same exponential equation (eq 1), implying no significant PPC effect.

All six PTCDI molecules employed in this work were found to form well-defined nanofibers, as evidenced in Figures S5a and S7 and our previous self-assembly studies.[27,34−36] The X-ray diffraction (XRD) patterns also indicate highly ordered 1D columnar microstructures, with the intercolumnar spacing determined by the well-defined peaks around 4.0°, to be 23.43, 21.08, 22.25, 27.35, 25.38, and 18.10 Å for MP-, MT-, MA-, MO-, DD-, and CH-PTCDI nanofibers, respectively (Figure S8).[35−38] However, the detailed molecule packing patterns are different as revealed by XRD patterns because the side group modification affects the molecular packing.[26,35,37] From our observation and results in Figure 3, it is unlikely that the different molecular packing or slight difference in morphology contributes significantly to the PPC. For example, even though DD-PTCDI and CH-PTCDI demonstrate great difference in molecular packing due to the side group effect (slipped stacking along the [100] direction for DD-PTCDI[39,40] vs flip-flap stacking for CH-PTCDI along the [100] direction[36]), none of them demonstrates significant PPC, implying that tuning the molecular packing does not likely produce PPC. Therefore, the observed PPC is more correlated with the donor−acceptor structure of PTCDI, which creates charge separation state through photoinduced electron transfer from the donor (the amine moiety) to acceptor (the PTCDI central core).[27,41] While the photoinduced electron transfer primarily occurs through an intramolecular process, it can also happen via an intermolecular process when the donor and acceptor are arranged in close proximity in the molecular assembly of nanofibers.[34,42,43] The charge separation between donor and acceptor can further be enhanced by the efficient electron delocalization along the $\pi-\pi$ stacking of PTCDI planes.[2,25,27,34,44] When the charge (negative or positive) is trapped at a molecule site, it may change the local dipole moment and the molecule orientation in the stacking as well, thus creating a local defect. It has also been widely argued in the literature that charge traps may come from the donors (acting as nucleophilic sites) and acceptors (as electrophilic sites) depending on the D−A association, which in turn can be controlled by the D−A strength and relative ratio of D and A moieties, as applied in memory devices.[45] The electrostatic potential fluctuation around the defect acts as an energy barrier

DOI: 10.1021/acsenergylett.6b00422
ACS Energy Lett. 2016, 1, 906−912

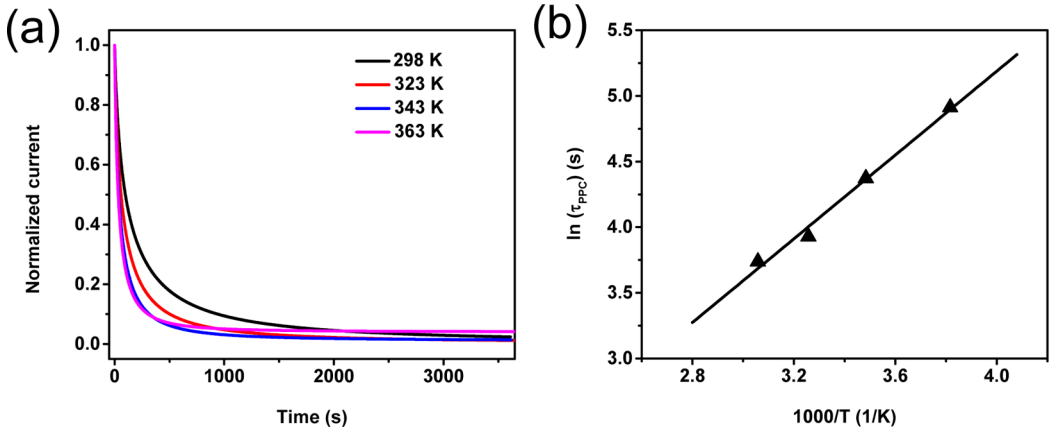

Figure 4. (a) PPC decay curves of MP-PTCDI nanofibers measured at different temperatures. (b) Logarithmic plot of the decay time constant as a function of reciprocal of temperature. The illumination power density was 3.50 mW cm^{-2}, and the bias voltage was 7 V.

preventing the charge recombination between electrons and holes, leading to PPC, similar to what was observed in inorganic semiconductor materials as described by the RLPF model.[11,14−18]

The photoinduced charge separation within the MP-PTCDI nanofibers can be confirmed by Kelvin probe force microscopy measurement (KPFM), which images the surface potential change of material caused by charge separation.[43,46,47] As shown in Figure S9a, well-defined morphology of the MP-PTCDI nanofibers was imaged by the tapping mode AFM. Panels b and d of Figure S9 show the surface potential images of MP-PTCDI nanofibers in the dark and after illumination, respectively. The statistic distributions of the relative surface potential measured accordingly are plotted in Figure S9c,e. Upon illumination, the surface potential of MP-PTCDI nanofibers became more negative (about −13 mV shift), indicating the significant charge separation driven by photoexcitation, which has been confirmed by the transient absorption spectral study.[48]

In addition to the photoinduced charge separation, strong electron donor can also initiate charge separation in the dark through steady-state charge-transfer interaction between the MP moiety (1-methylpiperidine moiety) on one molecule and the PTCDI part on the other molecule, as recently observed in our lab on the MP-PTCDI nanofibers[34] and other PTCDI materials.[44,49] The preformed charge carriers not only increase the electrical conductivity but meanwhile also create more structural defects that enhance the PPC, as discussed above. In contrast, the nanofibers of MA-PTCDI did not demonstrate such dark conductivity because of the lack of effective charge-transfer interaction between MA (*N*,*N*-dimethylaniline moiety) and PTCDI, and as a result, the PPC effect observed was minimal compared to that of MP-PTCDI (Figure 3) likely due to the intrinsically low density of defects in MA-PTCDI material. On the other hand, significant PPC was observed for the nanofibers of MT-PTCDI (Figure 3), which can be attributed to the high density of charge carriers in the steady state and the more defects thus created, similar to the case of MP-PTCDI. To confirm the steady-state charge transfer within MT-PTCDI nanofibers, we measured the fluorescence of both the molecular solution in chloroform (Figure S10) and the nanofibers deposited on quartz surface (Figure S11). The strong fluorescence measured for the MT-PTCDI molecules implies no photoinduced intramolecular electron transfer, which is consistent with the long donor−acceptor distance between the terminal amine and PTCDI.[27,34,50] However, when assembled into nanofibers, the MT-PTCDI molecules stack closely together, thus bringing the MT (*N*,*N*-dimethylbutylamine moiety) and PTCDI moieties in proximity, allowing for effective charge-transfer interaction, as supported by the complete fluorescence quenching in the nanofiber state (Figure S11). Such strong intermolecular charge-transfer interaction would increase the charge carrier density, as well as the defects that account for the significant PPC observed. The increased charge carrier density within MT-PTCDI nanofibers was also evidenced by the high dark current measured (0.008 μA at a bias of 7 V), which is comparable to that of MP-PTCDI nanofibers (0.010 μA at a bias of 7 V) but much higher than that of MA-PTCDI nanofibers (7.0×10^{-5} μA at a bias of 7 V), which were all measured under the same conditions.

According to the RLPF model,[11,14−18] we attribute the observed PPC in PTCDI nanofibers to the charge relevant defects, which generate a potential barrier preventing the recombination of photogenerated charge carriers. The potential barrier can be estimated from the temperature-dependent measurement of the PPC decay kinetics. Figure 4a shows the typical PPC decay curves measured on the MP-PTCDI nanofibers at different temperatures. It is clearly seen that the PPC effect gets more significant with a decrease in temperature. The decay time constants extracted from the curves show rapid decreasing at higher temperature (Figure S12). This temperature dependence indicates a typical thermally activated process for the charge recombination, which can be described by an Arrhenius equation (eq 2)[15,32]

$$\tau = \tau_0 \exp[\Delta E/k_B T] \quad (2)$$

where τ is the decay time constant at any experimental temperature, τ_0 the decay time constant at temperature of 0 K, ΔE the potential barrier of the charge recombination, k_B the Boltzmann constant, and T the temperature in the unit of Kelvin. Logarithmic plot of τ as a function of $1/T$ should give a linear relationship ($R^2 = 0.9840$) as indeed shown in Figure 4b. The slope of the linear fit gives the value of the potential barrier as 137 meV. This value is on the same level as those reported for n-type GaN.[15,18] This high activation barrier helps prevent the charge recombination, thereby enhancing the photovoltaic or photocatalytic efficiency when these PTCDIs are used as photoresponsive materials.

In conclusion, we have studied the PPC effect in PTCDI nanofiber materials. It was found that the PTCDIs containing

DOI: 10.1021/acsenergylett.6b00422
ACS Energy Lett. 2016, 1, 906−912

strong electron donor groups demonstrated significant PPC effect when fabricated into nanofiber materials. This is likely due to the defects formed from the charge separation within the molecular stacks, wherein the electrical potential barrier created around the defects prevents the recombination of the photogenerated charge carriers. The extended electron delocalization along the $\pi-\pi$ stacking (the long axis of nanofiber) further enhances the charge separation, creating more charge relevant defects, resulting in a more pronounced PPC. Because the charge recombination is typically a thermally activated process, the PPC shows strong temperature dependence. Linear fitting between the PPC decay time and temperature gives estimation of the activation barrier (energy), 137 meV, which is comparable to that obtained for the inorganic semiconductors such as n-type GaN. This work provides, for the first time, systematic investigations on the PPC effect in PTCDI-based materials (particularly the nanofibers), and the results will help understand the mechanism and design new material structures for sustained charge separation in order to further enhance the photovoltaic and photocatalytic efficiency of organic semiconductor materials.

■ ASSOCIATED CONTENT

Supporting Information

The Supporting Information is available free of charge on the ACS Publications website at DOI: 10.1021/acsenergylett.6b00422.

Experimental details, $I-V$ curves of all the PTCDI nanofibers in the dark and under illumination, UV−vis absorption of solid-state PTCDI nanofibers, summary of photocurrent on/off ratio and decay time constant of MP-PTCDI nanofibers under illumination with various irradiation power densities, wavelength-dependent photocurrent response, the decay time as a function of the molar amount of MP-PTCDI nanofibers deposited on the IDEs, SEM images of MP-PTCDI nanofibers in polymer matrix and its PPC relaxation curve, XRD patterns of PTCDI nanofibers, KPFM studies of MP-PTCDI nanofibers in the dark and after illumination, AFM images of MT-PTCDI nanofibers, UV−vis absorption and fluorescence spectra and images of MT-PTCDI in solution and solid state, and the decay time constant of MP-PTCDI nanofibers at different temperatures (PDF)

■ AUTHOR INFORMATION

Corresponding Author

*E-mail: lzang@eng.utah.edu.

Notes

The authors declare no competing financial interest.

■ ACKNOWLEDGMENTS

This work was supported by the Department of Homeland Security, Science and Technology Directorate under Grant 2009-ST-108-LR0005, NSF (CBET 1502433).

■ REFERENCES

(1) Chen, S.; Slattum, P.; Wang, C.; Zang, L. Self-Assembly of Perylene Imide Molecules into 1D Nanostructures: Methods, Morphologies, and Applications. *Chem. Rev.* **2015**, *115*, 11967−11998.

(2) Zang, L.; Che, Y.; Moore, J. S. One-Dimensional Self-Assembly of Planar π-Conjugated Molecules: Adaptable Building Blocks for Organic Nanodevices. *Acc. Chem. Res.* **2008**, *41*, 1596−1608.

(3) Hains, A. W.; Liang, Z.; Woodhouse, M. A.; Gregg, B. A. Molecular Semiconductors in Organic Photovoltaic Cells. *Chem. Rev.* **2010**, *110*, 6689−6735.

(4) Li, L.; Jacobs, D. L.; Bunes, B. R.; Huang, H.; Yang, X.; Zang, L. Anomalous High Photovoltages Observed in Shish Kebab-Like Organic p-n Junction Nanostructures. *Polym. Chem.* **2014**, *5*, 309−313.

(5) Kim, J. Y.; Bard, A. J. Organic Donor/Acceptor Heterojunction Photovoltaic Devices Based on Zinc Phthalocyanine and a Liquid Crystalline Perylene Diimide. *Chem. Phys. Lett.* **2004**, *383*, 11−15.

(6) Wicklein, A.; Ghosh, S.; Sommer, M.; Würthner, F.; Thelakkat, M. Self-Assembly of Semiconductor Organogelator Nanowires for Photoinduced Charge Separation. *ACS Nano* **2009**, *3*, 1107−1114.

(7) Chen, S.; Jacobs, D. L.; Xu, J.; Li, Y.; Wang, C.; Zang, L. 1D Nanofiber Composites of Perylene Diimides for Visible-Light-Driven Hydrogen Evolution from Water. *RSC Adv.* **2014**, *4*, 48486−48491.

(8) Chen, S.; Li, Y.; Wang, C. Visible-Light-Driven Photocatalytic H_2 Evolution from Aqueous Suspensions of Perylene Diimide Dye-Sensitized Pt/TiO_2 Catalysts. *RSC Adv.* **2015**, *5*, 15880−15885.

(9) Bu, L.; Pentzer, E.; Bokel, F. A.; Emrick, T.; Hayward, R. C. Growth of Polythiophene/Perylene Tetracarboxydiimide Donor/Acceptor Shish-Kebab Nanostructures by Coupled Crystal Modification. *ACS Nano* **2012**, *6*, 10924−10929.

(10) Chen, S.; Wang, C.; Bunes, B. R.; Li, Y.; Wang, C.; Zang, L. Enhancement of Visible-Light-Driven Photocatalytic H_2 Evolution from Water over g-C_3N_4 through Combination with Perylene Diimide Aggregates. *Appl. Catal., A* **2015**, *498*, 63−68.

(11) Wu, Y.-C.; Liu, C.-H.; Chen, S.-Y.; Shih, F.-Y.; Ho, P.-H.; Chen, C.-W.; Liang, C.-T.; Wang, W.-H. Extrinsic Origin of Persistent Photoconductivity in Monolayer MoS_2 Field Effect Transistors. *Sci. Rep.* **2015**, *5*, 11472.

(12) Mukherjee, B.; Sim, K.; Shin, T. J.; Lee, J.; Mukherjee, M.; Ree, M.; Pyo, S. Organic Phototransistors Based on Solution Grown, Ordered Single Crystalline Arrays of a π-Conjugated Molecule. *J. Mater. Chem.* **2012**, *22*, 3192−3200.

(13) Draper, E. R.; Walsh, J. J.; McDonald, T. O.; Zwijnenburg, M. A.; Cameron, P. J.; Cowan, A. J.; Adams, D. J. Air-Stable Photoconductive Films Formed from Perylene Bisimide Gelators. *J. Mater. Chem. C* **2014**, *2*, 5570−5575.

(14) Jiang, H. X.; Lin, J. Y. Persistent Photoconductivity and Related Critical Phenomena in $Zn_{0.3}Cd_{0.7}Se$. *Phys. Rev. B: Condens. Matter Mater. Phys.* **1989**, *40*, 10025−10028.

(15) Chen, H. M.; Chen, Y. F.; Lee, M. C.; Feng, M. S. Yellow Luminescence in n-Type GaN Epitaxial Films. *Phys. Rev. B: Condens. Matter Mater. Phys.* **1997**, *56*, 6942−6946.

(16) Dissanayake, A. S.; Huang, S. X.; Jiang, H. X.; Lin, J. Y. Charge Storage and Persistent Photoconductivity in a $CdS_{0.5}Se_{0.5}$ Semiconductor Alloy. *Phys. Rev. B: Condens. Matter Mater. Phys.* **1991**, *44*, 13343−13348.

(17) Roy, K.; Padmanabhan, M.; Goswami, S.; Sai, T. P.; Ramalingam, G.; Raghavan, S.; Ghosh, A. Graphene-MoS_2 Hybrid Structures for Multifunctional Photoresponsive Memory Devices. *Nat. Nanotechnol.* **2013**, *8*, 826−830.

(18) Hirsch, M. T.; Wolk, J. A.; Walukiewicz, W.; Haller, E. E. Persistent Photoconductivity in n-Type GaN. *Appl. Phys. Lett.* **1997**, *71*, 1098−1100.

(19) Lang, D. V.; Logan, R. A. Large-Lattice-Relaxation Model for Persistent Photoconductivity in Compound Semiconductors. *Phys. Rev. Lett.* **1977**, *39*, 635−639.

(20) Konstantatos, G.; Badioli, M.; Gaudreau, L.; Osmond, J.; Bernechea, M.; de Arquer, F. P. G.; Gatti, F.; Koppens, F. H. L. Hybrid Graphene-Quantum Dot Phototransistors with Ultrahigh Gain. *Nat. Nanotechnol.* **2012**, *7*, 363−368.

(21) Chen, S.-Y.; Lu, Y.-Y.; Shih, F.-Y.; Ho, P.-H.; Chen, Y.-F.; Chen, C.-W.; Chen, Y.-T.; Wang, W.-H. Biologically Inspired Graphene-Chlorophyll Phototransistors with High Gain. *Carbon* **2013**, *63*, 23−29.

DOI: 10.1021/acsenergylett.6b00422
ACS Energy Lett. 2016, 1, 906−912

(22) Dutta, S.; Narayan, K. S. Nonexponential Relaxation of Photoinduced Conductance in Organic Field Effect Transistors. *Phys. Rev. B: Condens. Matter Mater. Phys.* **2003**, *68*, 125208.
(23) Bubb, D. M.; O'Malley, S. M.; Antonacci, C.; Belmont, R.; McGill, R. A.; Crimi, C. Observation of Persistent Photoconductivity in Conducting Polyaniline Thin Films. *Appl. Phys. A: Mater. Sci. Process.* **2005**, *81*, 119−125.
(24) Nga Ng, T.; Fujieda, I.; Street, R. A.; Veres, J. Persistent Photoconductivity Effects in Printed n-Channel Organic Transistors. *J. Appl. Phys.* **2013**, *113*, 094506.
(25) Zang, L. Interfacial Donor−Acceptor Engineering of Nanofiber Materials to Achieve Photoconductivity and Applications. *Acc. Chem. Res.* **2015**, *48*, 2705−2714.
(26) Würthner, F. Perylene Bisimide Dyes as Versatile Building Blocks for Functional Supramolecular Architectures. *Chem. Commun.* **2004**, 1564−1579.
(27) Che, Y.; Yang, X.; Liu, G.; Yu, C.; Ji, H.; Zuo, J.; Zhao, J.; Zang, L. Ultrathin n-Type Organic Nanoribbons with High Photoconductivity and Application in Optoelectronic Vapor Sensing of Explosives. *J. Am. Chem. Soc.* **2010**, *132*, 5743−5750.
(28) Mateker, W. R.; Heumueller, T.; Cheacharoen, R.; Sachs-Quintana, I. T.; McGehee, M. D.; Warnan, J.; Beaujuge, P. M.; Liu, X.; Bazan, G. C. Molecular Packing and Arrangement Govern the Photo-Oxidative Stability of Organic Photovoltaic Materials. *Chem. Mater.* **2015**, *27*, 6345−6353.
(29) Sai, N.; Leung, K.; Zador, J.; Henkelman, G. First Principles Study of Photo-Oxidation Degradation Mechanisms in P3HT for Organic Solar Cells. *Phys. Chem. Chem. Phys.* **2014**, *16*, 8092−8099.
(30) Rivaton, A.; Tournebize, A.; Gaume, J.; Bussière, P.-O.; Gardette, J.-L.; Therias, S. Photostability of Organic Materials Used in Polymer Solar Cells. *Polym. Int.* **2014**, *63*, 1335−1345.
(31) Polenta, L.; Rossi, M.; Cavallini, A.; Calarco, R.; Marso, M.; Meijers, R.; Richter, T.; Stoica, T.; Lüth, H. Investigation on Localized States in GaN Nanowires. *ACS Nano* **2008**, *2*, 287−292.
(32) Lee, Y.-H.; Kang, J.-H.; Ryu, S.-W. Enhanced Photocurrent and Persistent Photoconductivity in Nanoporous GaN Formed by Electrochemical Etching. *Thin Solid Films* **2013**, *540*, 150−154.
(33) Datar, A.; Oitker, R.; Zang, L. Surface-Assisted One-Dimensional Self-Assembly of a Perylene Based Semiconductor Molecule. *Chem. Commun.* **2006**, 1649−1651.
(34) Wu, N.; Wang, C.; Bunes, B. R.; Zhang, Y.; Slattum, P. M.; Yang, X.; Zang, L. Chemical Self-Doping of Organic Nanoribbons for High Conductivity and Potential Application as Chemiresistive Sensor. *ACS Appl. Mater. Interfaces* **2016**, *8*, 12360−12368.
(35) Balakrishnan, K.; Datar, A.; Naddo, T.; Huang, J.; Oitker, R.; Yen, M.; Zhao, J.; Zang, L. Effect of Side-Chain Substituents on Self-Assembly of Perylene Diimide Molecules: Morphology Control. *J. Am. Chem. Soc.* **2006**, *128*, 7390−7398.
(36) Che, Y.; Yang, X.; Balakrishnan, K.; Zuo, J.; Zang, L. Highly Polarized and Self-Waveguided Emission from Single-Crystalline Organic Nanobelts. *Chem. Mater.* **2009**, *21*, 2930−2934.
(37) Jones, B. A.; Facchetti, A.; Wasielewski, M. R.; Marks, T. J. Tuning Orbital Energetics in Arylene Diimide Semiconductors. Materials Design for Ambient Stability of n-Type Charge Transport. *J. Am. Chem. Soc.* **2007**, *129*, 15259−15278.
(38) Huang, Y.; Fu, L.; Zou, W.; Zhang, F.; Wei, Z. Ammonia Sensory Properties Based on Single-Crystalline Micro/Nanostructures of Perylenediimide Derivatives: Core-Substituted Effect. *J. Phys. Chem. C* **2011**, *115*, 10399−10404.
(39) Bao, Q.; Goh, B. M.; Yan, B.; Yu, T.; Shen, Z.; Loh, K. P. Polarized Emission and Optical Waveguide in Crystalline Perylene Diimide Microwires. *Adv. Mater.* **2010**, *22*, 3661−3666.
(40) Briseno, A. L.; Mannsfeld, S. C. B.; Reese, C.; Hancock, J. M.; Xiong, Y.; Jenekhe, S. A.; Bao, Z.; Xia, Y. Perylenediimide Nanowires and Their Use in Fabricating Field-Effect Transistors and Complementary Inverters. *Nano Lett.* **2007**, *7*, 2847−2853.
(41) Zang, L.; Liu, R.; Holman, M. W.; Nguyen, K. T.; Adams, D. M. A Single-Molecule Probe Based on Intramolecular Electron Transfer. *J. Am. Chem. Soc.* **2002**, *124*, 10640−10641.
(42) Che, Y.; Huang, H.; Xu, M.; Zhang, C.; Bunes, B. R.; Yang, X.; Zang, L. Interfacial Engineering of Organic Nanofibril Heterojunctions into Highly Photoconductive Materials. *J. Am. Chem. Soc.* **2011**, *133*, 1087−1091.
(43) Huang, H.; Chou, C.-E.; Che, Y.; Li, L.; Wang, C.; Yang, X.; Peng, Z.; Zang, L. Morphology Control of Nanofibril Donor−Acceptor Heterojunction to Achieve High Photoconductivity: Exploration of New Molecular Design Rule. *J. Am. Chem. Soc.* **2013**, *135*, 16490−16496.
(44) Che, Y.; Datar, A.; Yang, X.; Naddo, T.; Zhao, J.; Zang, L. Enhancing One-Dimensional Charge Transport through Intermolecular π-Electron Delocalization: Conductivity Improvement for Organic Nanobelts. *J. Am. Chem. Soc.* **2007**, *129*, 6354−6355.
(45) Liu, C.-L.; Chen, W.-C. Donor-Acceptor Polymers for Advanced Memory Device Applications. *Polym. Chem.* **2011**, *2*, 2169−2174.
(46) Palermo, V.; Otten, M. B. J.; Liscio, A.; Schwartz, E.; de Witte, P. A. J.; Castriciano, M. A.; Wienk, M. M.; Nolde, F.; De Luca, G.; Cornelissen, J. J. L. M.; et al. The Relationship between Nanoscale Architecture and Function in Photovoltaic Multichromophoric Arrays as Visualized by Kelvin Probe Force Microscopy. *J. Am. Chem. Soc.* **2008**, *130*, 14605−14614.
(47) Liscio, A.; De Luca, G.; Nolde, F.; Palermo, V.; Müllen, K.; Samorì, P. Photovoltaic Charge Generation Visualized at the Nanoscale: A Proof of Principle. *J. Am. Chem. Soc.* **2008**, *130*, 780−781.
(48) Walsh, J. J.; Lee, J. R.; Draper, E. R.; King, S. M.; Jäckel, F.; Zwijnenburg, M. A.; Adams, D. J.; Cowan, A. J. Controlling Visible Light Driven Photoconductivity in Self-Assembled Perylene Bisimide Structures. *J. Phys. Chem. C* **2016**, *120*, 18479−18486.
(49) Arulkashmir, A.; Jain, B.; John, J. C.; Roy, K.; Krishnamoorthy, K. Chemically Doped Perylene Diimide Lamellae Based Field Effect Transistor with Low Operating Voltage and High Charge Carrier Mobility. *Chem. Commun.* **2014**, *50*, 326−328.
(50) Adams, D. M.; Brus, L.; Chidsey, C. E. D.; Creager, S.; Creutz, C.; Kagan, C. R.; Kamat, P. V.; Lieberman, M.; Lindsay, S.; Marcus, R. A.; et al. Charge Transfer on the Nanoscale: Current Status. *J. Phys. Chem. B* **2003**, *107*, 6668−6697.

DOI: 10.1021/acsenergylett.6b00422
ACS Energy Lett. 2016, 1, 906−912